ACS Energy LETTERS

Cite This: ACS Energy Lett. 2019, 4, 755−762

http://pubs.acs.org/journal/aelccp

LETTER

Efficient Trapping and Catalytic Conversion of Polysulfides by VS_4 Nanosites for Li−S Batteries

Sizhe Wang,[†,‡,⊥] Haiyuan Chen,[†,⊥] Jiaxuan Liao,[*,†] Qian Sun,[‡] Feipeng Zhao,[‡] Jing Luo,[‡] Xiaoting Lin,[‡] Xiaobin Niu,[†] Mengqiang Wu,[*,†] Ruying Li,[‡] and Xueliang Sun[*,‡]

[†]School of Materials and Energy, University of Electronic Science and Technology of China, Chengdu 611731, People's Republic of China

[‡]Department of Mechanical and Materials Engineering, University of Western Ontario, London, Ontario N6A 5B9, Canada

Supporting Information

ABSTRACT: Massive efforts have been devoted to enhancing performances of Li−S batteries to meet the requirements of practical applications. However, problems remain in enhancing the energy density and improving the cycle life. We present a free-standing structure of walnut-shaped VS_4 nanosites combine with carbon nanotubes (NTs) as cathodes. In this framework, NT arrays provide high surface area and conductivity for high sulfur loadings, and VS_4 nanosites facilitate trapping and catalytic conversions of lithium polysulfides. The synergistic effects of free-standing NT arrays and VS_4 nanosites have enabled high rate capability up to 6 C and long-term cycling with a low decay rate of 0.037% up to 1200 cycles at 2 C. Moreover, the designed cathode can achieve high areal capacities up to ∼13 mAh·cm^{-2} and estimated gravimetric energy density of 243.4 Wh·kg^{-1} at a system level, demonstrating great potential in practical applications of Li−S batteries.

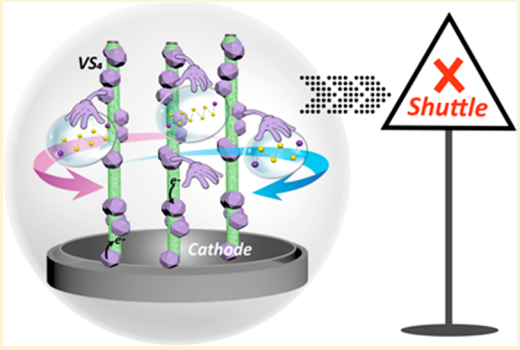

The lithium−sulfur (Li−S) battery shows great potential for next-generation energy storage devices owing to the high safety, low cost, and high energy density (∼2600 kW kg^{-1}).[1,2] However, the practical applications of Li−S batteries still need to handle two main issues of low energy density and poor cycle life on account of sulfur's low conductivity and lithium polysulfides' (LiPSs) shuttle reactions. Furthermore, low sulfur loading (<4 mg·cm^{-2}) and excessive usage of electrolyte (electrolyte/sulfur > 10 mL·mg^{-1}) also severely decrease the energy density at a system level.

To solve these problems, numerous structural designs are proposed to optimize specific components for Li−S batteries, including construction of efficient sulfur hosts for cathodes, interlayers, or surface coatings on separators, modifications of electrolyte composition, and protection of the lithium anodes.[3−5] Among the reported strategies, various carbon materials have been constructed to serve as conductive hosts for enhancing the cathode conductivity and sulfur utilization.[4] Conventionally, the sulfur cathodes are fabricated by the slurry casting method, where the poorly conductive polymer binders not only decrease the electronic conductivity of electrodes but also easily fail to maintain contact between active materials and substrates, particularly for the high-loading electrodes. Therefore, a three-dimensional (3D) free-standing conductive carbon-based matrix free of binder can be a promising sulfur host to enhance the integral conductivity and increase sulfur loadings.

However, simple carbon-based sulfur hosts cannot meet the requirement of long cycling stability, which is insufficient to alleviate the LiPS shuttles owing to weak van der Waals (vdW) interactions between polar LiPSs and nonpolar carbon-based materials.[6] Incorporation of polar materials into the carbon-based host enabling multifunctions of trapping and catalytic conversion of LiPSs is a promising approach to further improve the cycling ability.[7] Recently, various polar metal sulfides (MSs), such as MoS_2,[8,9] VS_x,[6,10−12] Sb_2S_3,[13] WS_2,[14] SnS_2,[15,16] and CoS_x,[17−21] have demonstrated great potential in alleviating the LiPSs' diffusion out of the sulfur hosts. VS_4, as a vanadium-based compound family member, was first discovered in 1906 and was illustrated in 1964 with specific crystal structure.[22,23] Different from the layer-type structure of VS_2, VS_4 has a chain-type structure of parallel quasi-one-dimensional chains of $V^{4+}(S_2^{2-})_2$, in which different chains bonded each other

Received: January 11, 2019
Accepted: February 20, 2019
Published: February 20, 2019

DOI: 10.1021/acsenergylett.9b00076
ACS Energy Lett. 2019, 4, 755−762

Scheme 1. Schematic Illustration of the Synthesis Process of the Free-Standing VS@NT Host

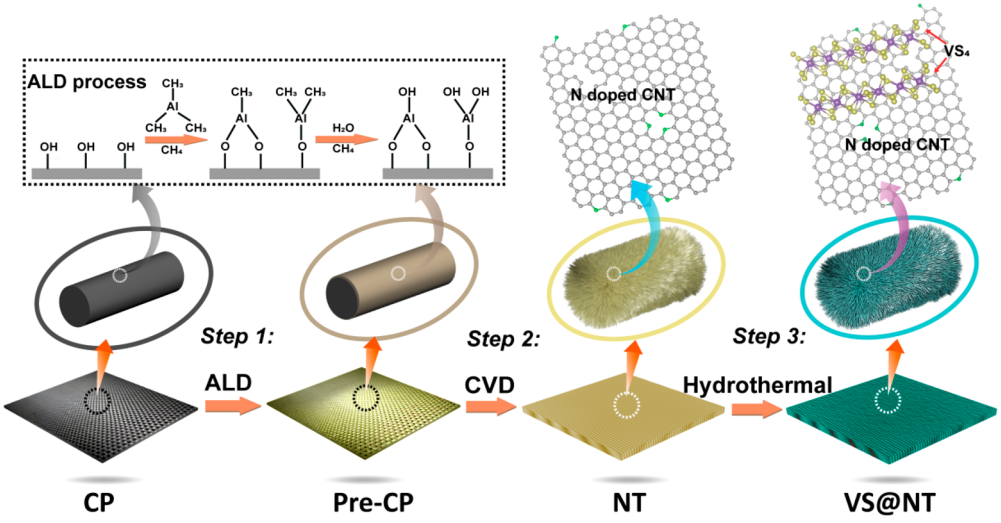

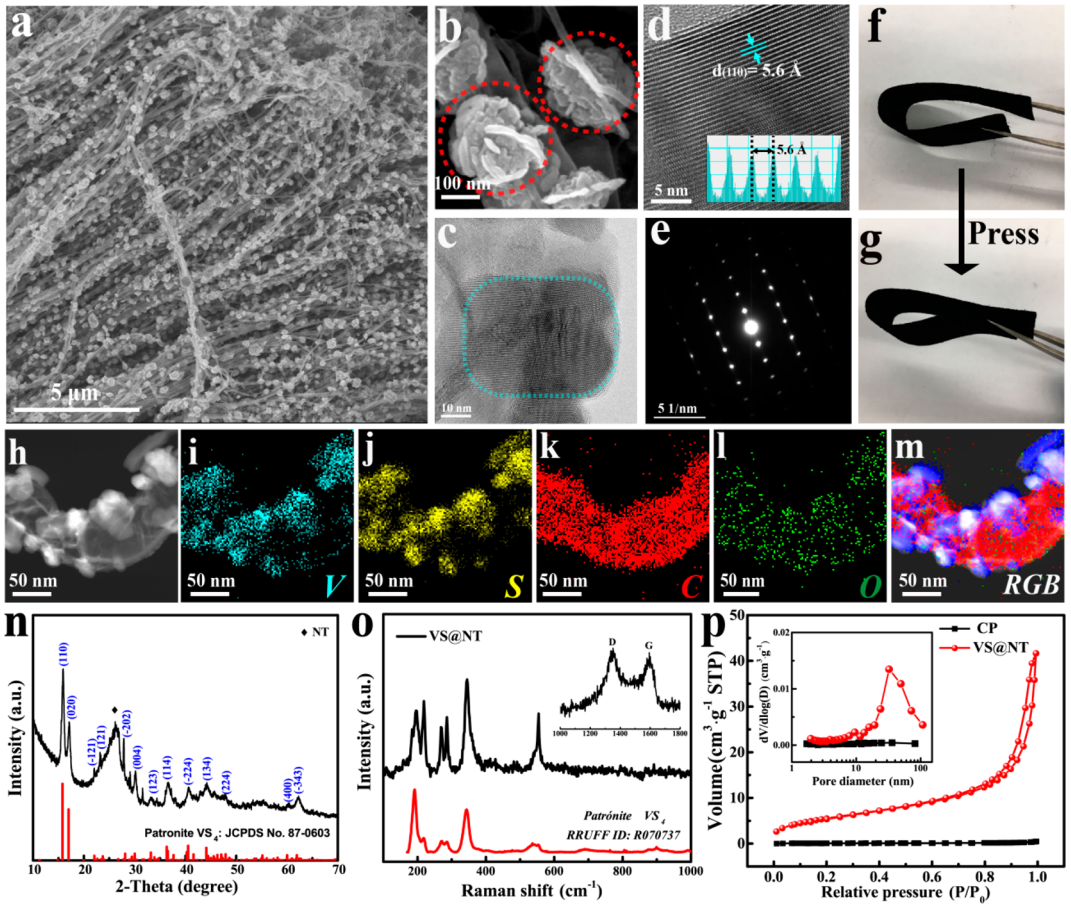

Figure 1. (a,b) SEM images; (c–e) TEM images and SAED pattern; (f,g) free-standing and flexible features; (h–m) EDX mapping images; (n) XRD patterns; and (o) Raman spectra of the VS@NT host. (p) N_2 adsorption–desorption curve analysis of the CP and VS@NT host (inset shows the corresponding pore size distribution curves).

through strong vdW interactions.[24,25] The polar LiPSs can potentially be trapped between the $V^{4+}(S_2^{2-})_2$ chains through even stronger vdW interactions than layer-type structure transition MSs.

On the basis of these considerations, on one hand, we designed nitrogen-doped carbon nanotube (NT) arrays paper as a 3D conductive host, which shows a large surface area to accommodate sulfur loading and high conductivity to promote the electron transfer. On the other hand, VS_4 nanoparticles are uniformly grown on the NT arrays (abbreviated as VS@NT) and serve as a mediator to trap and catalyze LiPS conversions. To the best of our knowledge, our work is the first demonstration of VS_4 as a catalytic mediator in Li–S battery cathodes. Through the synergistic effect of a free-standing NT

DOI: 10.1021/acsenergylett.9b00076
ACS Energy Lett. 2019, 4, 755–762

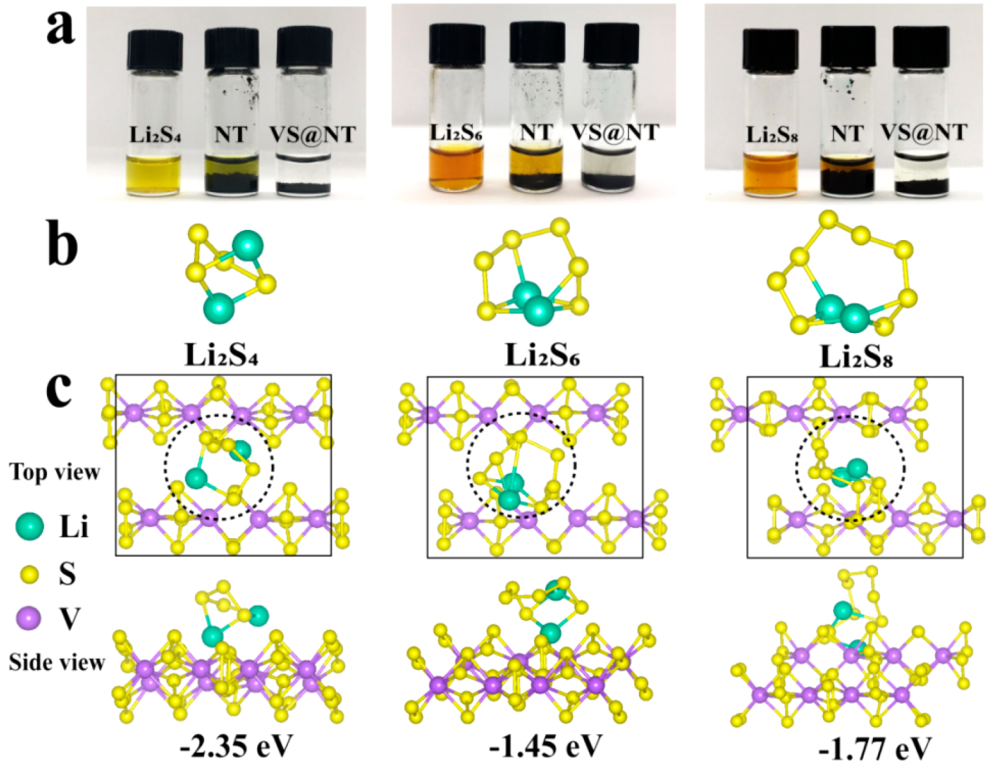

Figure 2. Adsorption test and theoretical DFT calculations of LiPS (Li_2S_4, Li_2S_6, Li_2S_8) adsorptions on VS@NT. (a) Optical photographs of LiPS trapping by NTs and VS@NTs, (b) DFT-calculated molecular structures of LiPSs, and (c) optimized configurations for the binding of LiPSs to the VS_4(110).

host and VS_4 nanosites, the VS@NT host achieved excellent electrochemical performance with high rate capability up to 6 C and outstanding long-term cycle ability with a low decay rate of 0.037% per cycle up to 1200 cycles at 2 C. Moreover, the cathode with a high areal capacity of ~13 mAh·cm^{-2} and corresponding gravimetric energy density of 243.4 Wh·kg^{-1} at a system level also demonstrate promise for practical applications.

VS@NT Synthesis and Characterizations. The synthesis process of the VS@NT free-standing host is illustrated in Scheme 1. First, aluminum was sputtered on the CP fibers as the buffer layer through an atomic layer deposition method. Second, NTs with an average diameter of ~50 nm and length of ~60 μm were grown radially on the CP fibers through a chemical vapor deposition process (Figure S1). Third, walnut-shaped VS_4 nanosites with an average particle size of ~160 nm were grown on the surface of NT uniformly (Figure 1a,b). The transmission electron microscopy (TEM) micrographs of VS@NT also showed an even dispersion of VS_4 nanosites on NTs, where the NT displayed bamboo-like features of hollow tubes with sectional joints (Figures 1c and S2). The *d*-spacing with clear lattice planes is ~0.56 nm (Figure 1d), indicating the (110) plane in a monoclinic crystal with the *Ic*/2 space group of VS_4, which is in accord with the selected-area electron diffraction pattern in Figure 1e.[25] The as-prepared VS@NT free-standing host was flexible and tolerant to bending (Figure 1f,g). In Figure 1h–m, the energy-dispersive X-ray elemental mappings confirmed that the ball-shaped particles grown on the NTs are derived from VS_4. The elemental mapping images of VS@NT at low magnification suggested a uniform concentration distribution of VS_4 nanosites across the electrode (Figure S3).

X-ray diffraction (XRD), Raman, and X-ray photoelectron spectroscopy (XPS) analyses were performed to analyze the details of the phase and composition of the VS@NT. As shown in the XRD pattern of VS@NT (Figure 1n), all of the main diffraction peaks agree well with the monoclinic phase VS_4 according to the JCPDS 87-0603. In Figure 1o, the three intensive Raman peaks at the fingerprints region of 150–400 cm^{-1} correspond to the patronite (VS_4 mineral) structure (RRUFF datebase: R070737). The D-band at ~1310 and G-band at ~1590 cm^{-1} correspond to defect-induced vibrations and sp^2 vibration in NT arrays.[26,27] The V 2p, S 2p, and C 1s XPS spectra are shown in Figure S4. The V 2p peaks at 516.7 and 524.4 eV are assigned to V^{4+} in VS_4.[28,29] The S 2p (2p3/2 and 2p3/1) peaks at 164.2 and 163.1 eV are assigned to S_2^{2-} 2p groups.[30] The nitrogen adsorption/desorption curves of the pure CP substrate and VS@NT host are shown in Figure 1p. The surface area of the CP substrate was only 0.32 m^2·g^{-1}. Notably, the surface area of VS@NT (20.6 m^2·g^{-1}) was more than 60 times larger than that of the pristine CP substrate. The substantially larger surface area can enable higher areal sulfur loadings.

LiPSs Trapping and Catalytic Conversions. In order to visualize the interactions between VS_4 and LiPSs, LiPS-containing (Li_2S_4, Li_2S_6, and Li_2S_8) solutions were prepared for adsorption tests (Figure 2a). The yellowish colors indicated the presence of LiPSs in the solutions. NTs and VS@NTs were added into the solutions separately. NTS exhibited negligible adsorption effects on LiPSs, as suggested by the minimal color change of solutions in the presence of NTS. In great contrast, all three LiPS-containing solutions became colorless after the addition of VS@NT, evidencing strong affinities and trapping capabilities of VS_4 for long-chain LiPSs, including Li_2S_4, Li_2S_6,

DOI: 10.1021/acsenergylett.9b00076
ACS Energy Lett. 2019, 4, 755–762

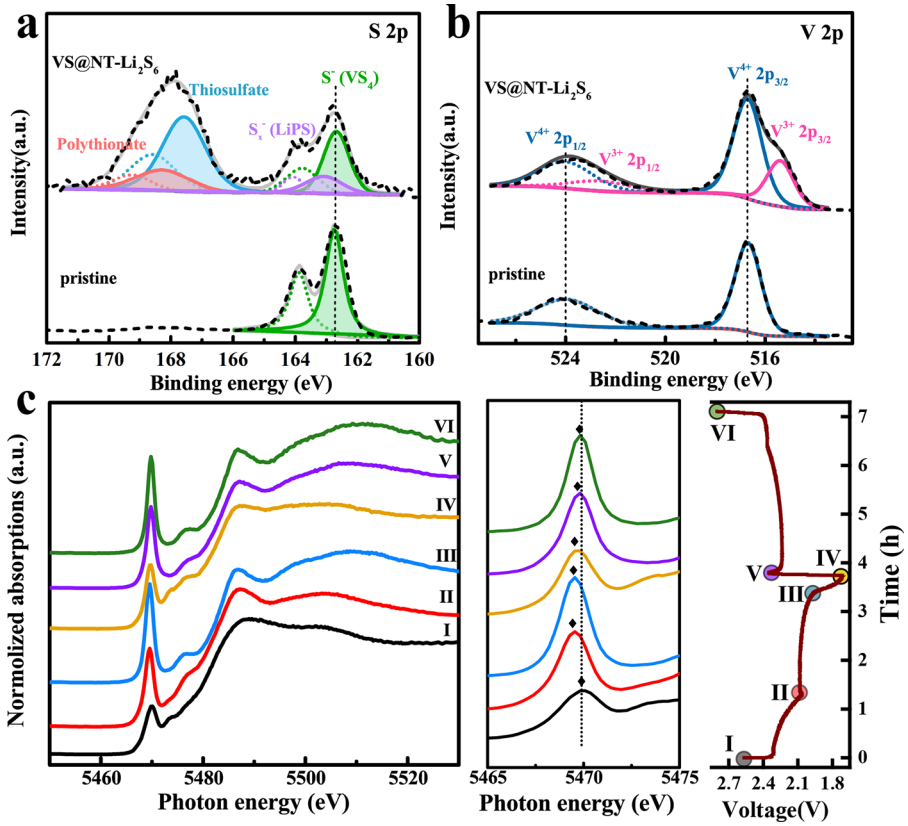

Figure 3. XPS spectrum of (a) S 2p and (b) V 2p peaks of pristine and VS@NT-Li_2S_6 samples; (c) XANES spectrum of the vanadium K-edge for the VS@NT/S cathode at certain states of charge/discharge during the first cycle and corresponding enlarged part of the pre-edge between 5465 and 5475 eV ((I) pristine VS@NT, (II) discharge to 2.1 V, (III) discharge to 2.0 V, (IV) discharge to 1.7 V, (V) charge to 2.3 V, and (VI) charge to 2.8 V).

and Li_2S_8. This phenomenon is further confirmed by the UV−vis curves of Li_2S_6 solution before/after adding VS@NT (Figure S5). In the region of 400−500 nm, the strong absorbance is clearly observed and derived from the Li_2S_6 in solutions. However, after adding VS@NT into Li_2S_6 solutions for a period of time, the absorbance significantly decreased and there was no obvious absorbance peak.

The chemical interactions between VS_4 and long-chain LiPSs (Li_2S_n, n = 4, 6, 8) were elucidated using density functional theory (DFT) calculations. The LiPS adsorption on VS_4 nanosites via strong vdW interactions between the $V^{4+}(S_2^{2-})_2$ chains and LiPS species were considered. The molecular structures of Li_2S_4, Li_2S_6, and Li_2S_8 are shown in Figure 2b. The optimized LiPS geometries on VS_4(110) are shown in Figure 2c. The absorption energies between VS_4 and Li_2S_4, Li_2S_6, and Li_2S_8 are calculated to be −2.35, −1.45, and −1.77 eV, respectively. Owing to the unique chain-type structure of VS_4, the absorption energies between VS_4 and LiPSs are not only much larger than the nonpolar carbon materials (such as graphene,[31] NTs[32]) but also comparable to those of most of the transition metal dichalcogenides (such as VS_2, MoS_2, WS_2, NbS_2, TiS_2, ZrS_2[14,33,34]) and some other vanadium-based oxides (such as VO_2,[35,36] V_2O_3,[37] V_2O_5[33]), which effectively facilitate trapping of LiPSs.

To further identify the catalytic conversions of LiPSs by VS_4, symmetrical cells with two identical electrodes, either NTs or VS@NTs, were tested with cyclic voltammetry (CV) analyses (Figure S6). The electrolytes with or without addition of Li_2S_6 were compared. For symmetric cells without Li_2S_6, the current densities of both VS@NT and NT cells were negligible. It is indicated that the capacitive currents were mainly derived from the redox reaction from Li_2S_6.[18,38] In the presence of Li_2S_6, the current polarization of the VS@NT cell was much larger than that of the NT cell, demonstrating that VS_4 is not only able to electrochemically trap the LiPSs but also to catalyze reversible conversions of LiPSs. To further demonstrate the superiority of the VS@NT host in regard to the Li_2S precipitation process, discharge curves of a Li_2S_8 solution at potentiostatic 2.05 V were collected for NT and VS@NT cells using Li metal as the counter electrode (Figure S7). Compared with the NT host (~29.3 mAh·g^{-1}), the capacity of Li_2S precipitation on the VS@NT host was almost 10 times larger (~260.4 mAh·g^{-1}) based on Faraday's law.[39] The effective catalytic effect of VS_4 on LiPSs conversion was clearly demonstrated.

We used a Li_2S_6 solution without adding LiTFSI and $LiNO_3$ as a representation of LIPS to detect the catalytic reaction products with VS_4. After soaking the VS@NT host in Li_2S_6 solution, the S_x^- 2p peaks (derived from the LiPSs) appeared at a higher binding energy (Figure 3a). Also, the typical S 2p peaks of thiosulfate ($S_2O_3^{2-}$) and polythionate complexes ($[O_3S_2-(S)^x-S_2O_3]$) appeared at 167.6 eV (2p 1/2 168.6 eV) and 168.3 eV (2p 1/2169.4 eV), which were derived from the oxidization of the LiPSs catalyzed with VS_4 nanosites. By this means, the surface-formed $S_2O_3^{2-}$ complex will work as an mediator to react with LiPSs and for catalytic conversion to insoluble Li_2S_2/Li_2S.[40] Accordingly, except for the V^{4+} derived from the pristine VS_4, obvious V^{3+} 2p peaks appeared at 515.4 and 522.7 eV (Figure 3b), which further testify to the redox

DOI: 10.1021/acsenergylett.9b00076
ACS Energy Lett. 2019, 4, 755−762

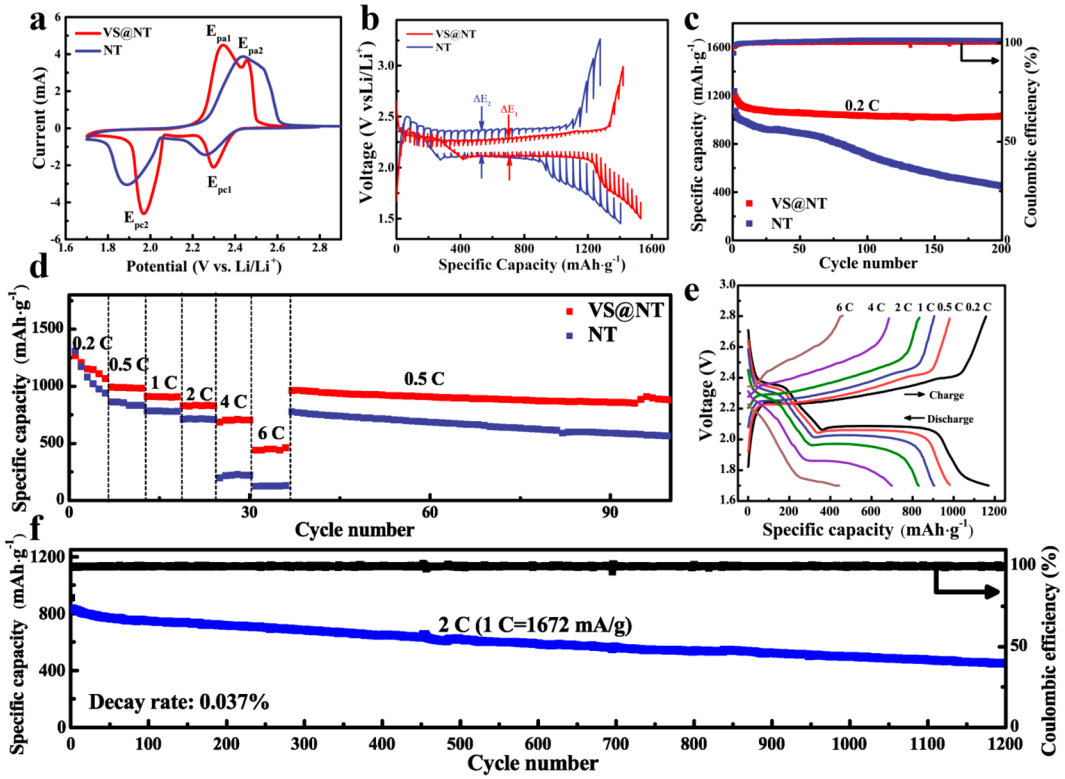

Figure 4. (a) CV curves at a scanning rate of 0.2 mV·s^{-1}; (b) GITT curves of the charge/discharge process; (c) cyclic performance at 0.2 C for 200 cycles; (d) rate performance at various current densities from 0.2 to 6 C of NT/S and VS@NT/S cathodes; (e) corresponding galvanostatic charge/discharge curves at different current rates; (f) long-term cycling performance at 2 C of the VS@NT/S cathode.

reaction between VS_4 and LiPSs. To further detect the reaction mechanism between VS_4 nanosites and LiPSs, X-ray absorption near-edge spectroscopy (XANES) at different charge/discharge states in the first cycle was used to determine the variations of the V K-edge (Figure 3c). The pre-edge of the V K-edge in the enlarged part shifts back to the lower-energy position during the discharge process and then shifts back to a similar position after a charge process, which strongly identifies the reversibility of VS_4 as a catalyst to trap and catalyze conversion of LiPSs.

Electrochemical Performance. By drop-casting different volumes of sulfur-containing solutions, VS@NTs and NTs with different sulfur loadings (named VS@NT/S and NT/S cathodes) were obtained. The CV curves of the VS@NT/S and NT/S cathodes scanned between 1.7 and 2.8 V at a rate of 0.1 mV·s^{-1} are shown in Figure 4a. The corresponding peak potentials are summarized in Figure S8. The peaks in the CV curves correspond to the voltage plateaus of galvanostatic charge/discharge profiles. The redox peaks of the VS@NT/S cell were much sharper and higher than those of the NT/S cell, which indicates faster kinetics of the VS@NT/S cell for Li-ion diffusion across the cathode material. Compared to the peaks of the NT/S cell, the discharge peaks of the VS@NT/S cell shift to higher potentials (from 1.89 and 2.26 V to 1.97 and 2.30 V), and the charge peaks of the VS@NT/S cell shift to a lower potential (from 2.43 and 2.53 V to 2.34 and 2.46 V). The significantly reduced polarization also indicated improved redox kinetics by VS_4 during cycling.[41] The galvanostatic intermittent titration technique (GITT) curves of VS@NT/S and NT/S cathodes are measured under almost quasi-equilibrium conditions (Figures 4b and S9). In the initial charging process, the VS@NT/S cathode delivers a lower potential barrier than that of the NT/S cathode, indicating an accelerated activation process with low charge transfer resistance.[42] Compared with the NT/S cell, the charge/discharge plateaus of VS@NT/S were extended with reduced polarizations, leading to a larger capacity and higher energy efficiency. In addition, VS@NT/S with a decreased voltage gap (between charge and discharge plateaus) indicates the decreased hysteresis,[43] which again confirms the accelerated redox kinetics by VS@NT/S. The impedance of the VS@NT/S cell before and after cycling was also consistently smaller than that of the NT/S cell (Figure S10).[42]

In Figure 4c, the cycling performances of the VS@NT/S and NT/S cathodes were compared at a current density of 0.2 C (1 C = 1672 mA·g^{-1}). The VS@NT/S cathode delivered a high reversible capacity of ~1100 mAh·g^{-1} with stable cyclic performance at 0.2 C for 200 cycles. The VS@NT cell without S loading was also tested to measure the contribution of VS_4 (Figure S11). The reversible capacity from a catalyst of VS_4 is only about 50 mAh·g^{-1}, which is so small that it could be neglected and hinder further identification of the real capacity contribution from sulfur. Without further protection on the lithium metal anode, a high Coulombic efficiency of ~100% was maintained, again confirming the excellent confinement of the LiPS intermediate on the cathode side. In comparison, the capacity of the NT/S cathode faded gradually with a capacity retention of only 43% after 200 cycles (compared to the second cycle). The rate capabilities of the VS@NT/S and NT/S cathodes tested at rates between 0.2 and 6 C are shown in Figure 4d. The average reversible capacities of the VS@NT/S cell are 1154, 988, 906, 832, 709, and 451 mAh·g^{-1} at rates of 0.2, 0.5, 1, 2, 4, and 6 C, respectively. The capacities were highly stable at each current density. However, the NT/S cell

DOI: 10.1021/acsenergylett.9b00076
ACS Energy Lett. 2019, 4, 755−762

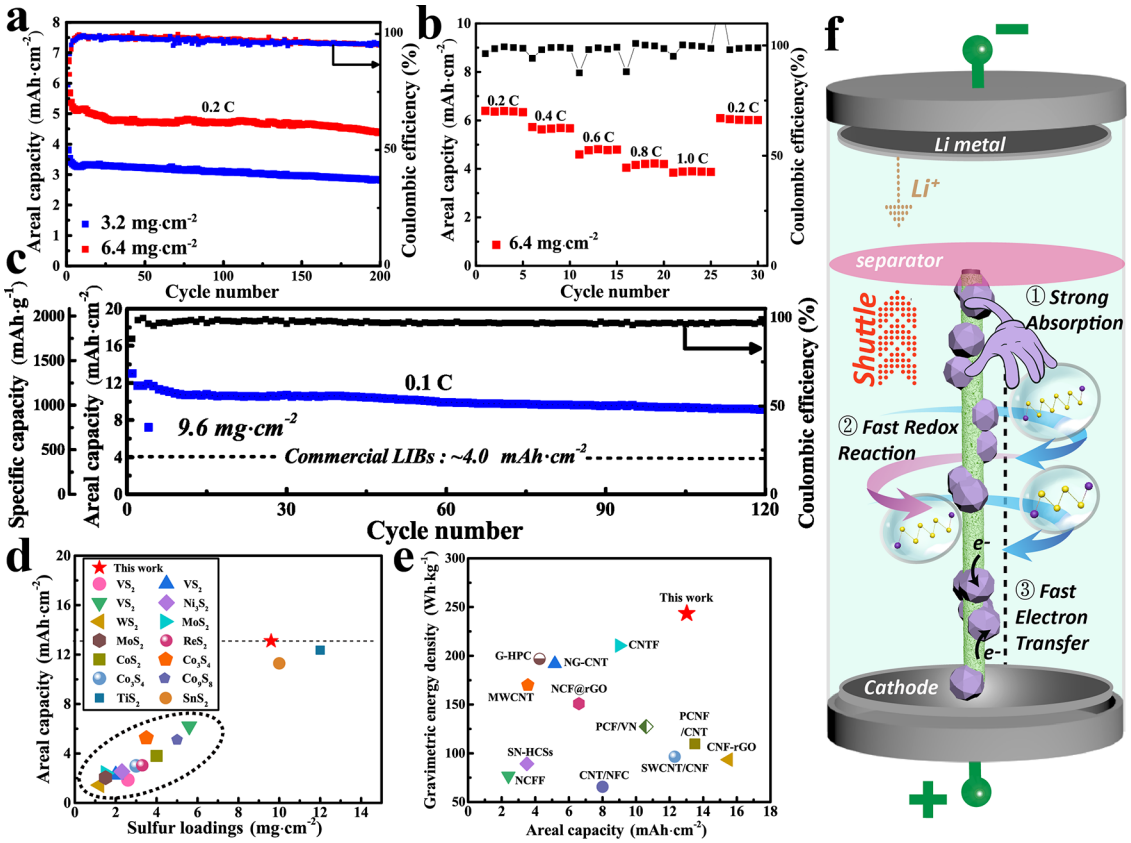

Figure 5. (a) Cycling performance of VS@NT/S cathodes with sulfur loadings of 3.2 and 6.4 mg·cm^{-2} at 0.2 C for 200 cycles; (b) rate capability curves of VS@NT cathodes with sulfur loadings of 6.4 mg·cm^{-2} at various current densities from 0.2 to 1 C; (c) cycling performance of the VS@NT/S cathode with sulfur loadings of 9.6 mg·cm^{-2} at 0.1 C for 120 cycles; (d) performance comparisons with recent works on MS-based materials as Li−S battery cathodes; (e) performance comparisons with recent works on free-standing high sulfur loading Li−S batteries cathodes; (f) schematic illustration of confinement and catalytic conversion of LiPSs by the VS@NT host in a Li−S battery model.

showed poor rate performance with average reversible capacities of only 225 and 128 mAh·g^{-1} at rates of 4 and 6 C. The corresponding galvanostatic charge/discharge curves are shown in Figures 4e and S12. The NT/S cell failed to maintain the second discharge plateau at rates of 4 and 6 C due to the inherently large polarization upon increasing current rates. The enhanced rate performance of VS@NT indicated that the VS_4 nanosites effectively promote the improvement of rate performance.

To evaluate stability in long-term cycling of the VS@NT/S cathode, the cell was tested at 2 C for 1200 cycles (Figure 4f). The cell performed an ultralow capacity decay rate of 0.037% per cycle in the long-term cycling of 1200 cycles. A high reversible capacity of 455 mAh·g^{-1} was obtained even after 1200 cycles. The separators after long-term cycling were obtained by disassembling the cells (Figure S13). The separators with distinct differences in color verified that LiPSs was effectively confined by VS@NT without excessive dissolving into the electrolyte.

In this context, the cycling and rate performances of VS@NT/S cathodes with high sulfur loadings of 3.2, 6.4, 9.6, 13.3, 16 mg cm^{-2} were further investigated. In Figure 5a, the VS@NT/S cathode with sulfur loadings of 3.2 and 6.4 mg cm^{-2} shows initial areal capacities of 3.8 and 6.7 mAh cm^{-2} at 0.2 C, respectively. After 200 cycles, the cathodes with sulfur loadings of 3.2 and 6.4 mg cm^{-2} retain areal capacities of 2.9 and 4.2 mAh cm^{-2}, accounting for 83.0 and 77.6% (compared to the second cycle), respectively. Figure S14 shows the SEM images of VS@NT/S after 200 cycles at 0.2 C. The high-loading VS@NT/S cathodes after cycling still maintain the analogous structure of VS_4 nanosites on NTs, which indicates that the 3D structure VS@NT host has high structural stability. No obvious reaction side products were observed. The rate capability of the 6.4 mg·cm^{-2} VS@NT/S cathode was also tested (Figure 5b). The average reversible capacities of VS@NT/S cathodes are 6.3, 5.7, 4.8, 4.2, and 3.9 mAh cm^{-2} (corresponding capacities are 990, 886, 748, 655, and 604 mAh·g^{-1}) at rates of 0.2, 0.4, 0.6, 0.8, and 1 C, respectively, which suggests that the incorporation of VS_4 could effectively enhance the rate performance even with high sulfur loadings.

The electrochemical performance of the VS@NT/S cathode with a sulfur areal loading of 9.6 mg·cm^{-2} was also tested (Figure 5c). The VS@NT/S cell at 0.1 C showed a high initial specific capacity of 1356 mAh·g^{-1} and high initial areal capacities of 13.0 mAh·cm^{-2}, implying a high sulfur utilization of ~80% enabled by the VS@NT conductive networks. The VS@NT/S cathode of 9.6 mg·cm^{-2} maintains a high specific capacity of 952 mAh·g^{-1} and high areal capacity of 9.1 mAh·cm^{-2} even after 120 cycles (capacity retention is 78.1% based on the second cycle), which is much higher than that of the commercial lithium-ion batteries (4 mAh·cm^{-2}). The sulfur loading was optimized at ~10 mg cm^{-2} for the VS@NT host because further increase in sulfur loading to 13.3 and 16 mg·cm^{-2} led to a decrease in areal capacities (Figure S15).

DOI: 10.1021/acsenergylett.9b00076
ACS Energy Lett. 2019, 4, 755−762

Nevertheless, the VS@NT/S cathode of 13.3 and 16 mg·cm^{-2} still could maintain stable cycling but lower specific capacities and sulfur utilization. Compared with recent works on MS-based electrodes for Li−S batteries, our work achieved one of the best performances among them as of yet (Figure 5d and details in Table S1). More importantly, gravimetric energy densities (243.4 Wh kg^{-1}) at a system level (considering the total mass of the cathode, electrolyte, separator, and Li metal) were achieved for the VS@NT-based Li−S battery, which shows competitive performance among the recently reported high-loading free-standing Li−S battery cathodes (Figure 5e and Table S2).

A schematic illustration of confinement and catalytic conversion of LiPSs by a VS@NT cathode in a Li−S battery model is shown in Figure 5f. First, NT arrays with a large surface area help to enhance the sulfur loading with uniform distribution; second, the NT arrays provide fast electron transfer pathways for high rate capability; third, the VS_4 nanosites on the NT serve as a strong trapping mediator to absorb the LiPSs with strong chemical interaction. Moreover, the VS_4 nanosites promote catalytic conversions between LiPSs and the insoluble Li_2S reduction end product with fast redox kinetics, not only restraining LiPSs dissolution in the electrolyte but also further improving high rate capabilities. On the basis of these fascinating structural characters and excellent electrochemical performances, the VS@NT/S cathode manifests the great potential of the VS@NT/S in pursuing high energy density and long cycling life Li−S batteries for next-generation energy storage applications.

We proposed a 3D free-standing cathode consisting of walnut-shaped VS_4 nanosites grown on radial NT arrays. In the designed electrode, NT arrays provide a large surface area for high sulfur loading and fast electron transfer pathways between sulfur and the host. More importantly, the VS_4 nanosites work as a reversible catalyst to trap and catalyze conversion from soluble LiPSs to insoluble Li_2S, which effectively suppresses the shuttle reaction for stable cycling life. These structural superiorities of the VS@NT composite host endow high-performance sulfur cathodes with high areal capacity, high rate capability, and excellent cyclability, demonstrating great promise in developing high energy density Li−S batteries for future practical applications.

■ ASSOCIATED CONTENT

Supporting Information

The Supporting Information is available free of charge on the ACS Publications website at DOI: 10.1021/acsenergylett.9b00076.

Experiment and calculation details, SEM and TEM images, EDX mappings, XPS, UV−vis, CV, EIS, GITT, discharge/charge curves, cycling performances, and two tables summarizing the electrochemical properties of electroactive material composites (PDF)

■ AUTHOR INFORMATION

Corresponding Authors

*E-mail: jxliao@uestc.edu.cn (J.L.).
*E-mail: mwu@uestc.edu.cn (M.W.).
*E-mail: xsun@eng.uwo.ca (X.S.).

ORCID

Sizhe Wang: 0000-0002-2068-6308
Jiaxuan Liao: 0000-0002-8094-5500
Xiaobin Niu: 0000-0003-0717-6810
Mengqiang Wu: 0000-0002-0624-4335
Xueliang Sun: 0000-0003-2881-8237

Author Contributions

⊥S.Z.W. and H.Y.C. contributed equally to this work.

Notes

The authors declare no competing financial interest.

■ ACKNOWLEDGMENTS

This research was supported by the Natural Science and Engineering Research Council of Canada (NSERC), the Canada Research Chair Program (CRC), the Canada Foundation for Innovation (CFI), the Western University, National Natural Science Foundations of China of 51172034, the National Defense Science and technology innovation special zone project of 17-163-13-ZT-009-125-001, and the International cooperation projects of Sichuan Provincial Department of science and technology of 2017HH0067 and 2017HH0101. S.W. is supported by the Chinese Scholarship Council. The authors also acknowledge technical support from the Canadian Centre of Electron Microscopy (CCEM) at McMaster University for the TEM characterizations.

■ REFERENCES

(1) Peng, H.-J.; Huang, J.-Q.; Cheng, X.-B.; Zhang, Q. Review on High-Loading and High-Energy Lithium-Sulfur Batteries. *Adv. Energy Mater.* **2017**, *7*, 1700260.

(2) Yang, X.; Li, X.; Adair, K.; Zhang, H.; Sun, X. Structural Design of Lithium−Sulfur Batteries: From Fundamental Research to Practical Application. *Electrochemical Energy Reviews* **2018**, *1*, 239−293.

(3) Li, Q.; Song, Y.; Xu, R.; Zhang, L.; Gao, J.; Xia, Z.; Tian, Z.; Wei, N.; Rummeli, M. H.; Zou, X.; et al. Biotemplating Growth of Nepenthes-like N-Doped Graphene as a Bifunctional Polysulfide Scavenger for Li-S Batteries. *ACS Nano* **2018**, *12*, 10240−10250.

(4) Seh, Z. W.; Sun, Y.; Zhang, Q.; Cui, Y. Designing high-energy lithium-sulfur batteries. *Chem. Soc. Rev.* **2016**, *45*, 5605−5634.

(5) Luo, J.; Lee, R. C.; Jin, J. T.; Weng, Y. T.; Fang, C. C.; Wu, N. L. A dual-functional polymer coating on a lithium anode for suppressing dendrite growth and polysulfide shuttling in Li-S batteries. *Chem. Commun.* **2017**, *53*, 963−966.

(6) Zhu, X.; Zhao, W.; Song, Y.; Li, Q.; Ding, F.; Sun, J.; Zhang, L.; Liu, Z. In Situ Assembly of 2D Conductive Vanadium Disulfide with Graphene as a High-Sulfur-Loading Host for Lithium-Sulfur Batteries. *Adv. Energy Mater.* **2018**, *8*, 1800201.

(7) Liu, D.; Zhang, C.; Zhou, G.; Lv, W.; Ling, G.; Zhi, L.; Yang, Q. H. Catalytic Effects in Lithium-Sulfur Batteries: Promoted Sulfur Transformation and Reduced Shuttle Effect. *Adv. Sci. (Weinh)* **2018**, *5*, 1700270.

(8) Lin, H.; Yang, L.; Jiang, X.; Li, G.; Zhang, T.; Yao, Q.; Zheng, G. W.; Lee, J. Y. Electrocatalysis of polysulfide conversion by sulfur-deficient MoS_2 nanoflakes for lithium−sulfur batteries. *Energy Environ. Sci.* **2017**, *10*, 1476−1486.

(9) Tang, W.; Chen, Z.; Tian, B.; Lee, H. W.; Zhao, X.; Fan, X.; Fan, Y.; Leng, K.; Peng, C.; Kim, M. H.; et al. In Situ Observation and Electrochemical Study of Encapsulated Sulfur Nanoparticles by MoS_2 Flakes. *J. Am. Chem. Soc.* **2017**, *139*, 10133−10141.

(10) Cheng, Z.; Xiao, Z.; Pan, H.; Wang, S.; Wang, R. Elastic Sandwich-Type rGO-VS_2/S Composites with High Tap Density: Structural and Chemical Cooperativity Enabling Lithium-Sulfur Batteries with High Energy Density. *Adv. Energy Mater.* **2018**, *8*, 1702337.

(11) Wang, L.; He, Y.-B.; Shen, L.; Lei, D.; Ma, J.; Ye, H.; Shi, K.; Li, B.; Kang, F. Ultra-small self-discharge and stable lithium-sulfur batteries achieved by synergetic effects of multicomponent sandwich-type composite interlayer. *Nano Energy* **2018**, *50*, 367−375.

DOI: 10.1021/acsenergylett.9b00076
ACS Energy Lett. 2019, 4, 755−762

(12) Wang, M.; Fan, L.; Qiu, Y.; Chen, D.; Wu, X.; Zhao, C.; Cheng, J.; Wang, Y.; Zhang, N.; Sun, K. Electrochemically active separators with excellent catalytic ability toward high-performance Li−S batteries. *J. Mater. Chem. A* **2018**, *6*, 11694−11699.
(13) Yao, S.; Cui, J.; Huang, J.-Q.; Lu, Z.; Deng, Y.; Chong, W. G.; Wu, J.; Ihsan Ul Haq, M.; Ciucci, F.; Kim, J.-K. Novel 2D Sb_2S_3 Nanosheet/CNT Coupling Layer for Exceptional Polysulfide Recycling Performance. *Adv. Energy Mater.* **2018**, *8*, 1800710.
(14) Lei, T.; Chen, W.; Huang, J.; Yan, C.; Sun, H.; Wang, C.; Zhang, W.; Li, Y.; Xiong, J. Multi-Functional Layered WS_2 Nanosheets for Enhancing the Performance of Lithium-Sulfur Batteries. *Adv. Energy Mater.* **2017**, *7*, 1601843.
(15) Luo, L.; Chung, S.-H.; Manthiram, A. A three-dimensional self-assembled SnS_2-nano-dots@graphene hybrid aerogel as an efficient polysulfide reservoir for high-performance lithium−sulfur batteries. *J. Mater. Chem. A* **2018**, *6*, 7659−7667.
(16) Gao, X.; Yang, X.; Li, M.; Sun, Q.; Liang, J.; Luo, J.; Wang, J.; Li, W.; Liang, J.; Liu, Y.; et al. Cobalt-Doped SnS_2 with Dual Active Centers of Synergistic Absorption-Catalysis Effect for High-S Loading Li−S Batteries. *Adv. Funct. Mater.* **2019**, *29*, 1806724.
(17) Ma, L.; Zhang, W.; Wang, L.; Hu, Y.; Zhu, G.; Wang, Y.; Chen, R.; Chen, T.; Tie, Z.; Liu, J.; et al. Strong Capillarity, Chemisorption, and Electrocatalytic Capability of Crisscrossed Nanostraws Enabled Flexible, High-Rate, and Long-Cycling Lithium-Sulfur Batteries. *ACS Nano* **2018**, *12*, 4868−4876.
(18) Yuan, Z.; Peng, H. J.; Hou, T. Z.; Huang, J. Q.; Chen, C. M.; Wang, D. W.; Cheng, X. B.; Wei, F.; Zhang, Q. Powering Lithium-Sulfur Battery Performance by Propelling Polysulfide Redox at Sulfiphilic Hosts. *Nano Lett.* **2016**, *16*, 519−527.
(19) Pu, J.; Shen, Z.; Zheng, J.; Wu, W.; Zhu, C.; Zhou, Q.; Zhang, H.; Pan, F. Multifunctional Co_3S_4@sulfur nanotubes for enhanced lithium-sulfur battery performance. *Nano Energy* **2017**, *37*, 7−14.
(20) Chen, T.; Ma, L.; Cheng, B.; Chen, R.; Hu, Y.; Zhu, G.; Wang, Y.; Liang, J.; Tie, Z.; Liu, J.; et al. Metallic and polar Co_9S_8 inlaid carbon hollow nanopolyhedra as efficient polysulfide mediator for lithium−sulfur batteries. *Nano Energy* **2017**, *38*, 239−248.
(21) Dai, C.; Lim, J.-M.; Wang, M.; Hu, L.; Chen, Y.; Chen, Z.; Chen, H.; Bao, S.-J.; Shen, B.; Li, Y.; et al. Honeycomb-Like Spherical Cathode Host Constructed from Hollow Metallic and Polar Co_9S_8 Tubules for Advanced Lithium-Sulfur Batteries. *Adv. Funct. Mater.* **2018**, *28*, 1704443.
(22) Hillebrand, W. THE VANADIUM SULPHIDE, PATRONITE, AND ITS MINERAL ASSOCIATES FROM MINASRAGRA, PERU. *J. Am. Chem. Soc.* **1907**, *29*, 1019−1029.
(23) Allmann, R.; Baumann, I.; Kutoglu, A.; Rösch, H.; Hellner, E. Die Kristallstruktur des Patronits $V(S_2)_2$. *Naturwissenschaften* **1964**, *51*, 263−264.
(24) Rout, C. S.; Kim, B. H.; Xu, X.; Yang, J.; Jeong, H. Y.; Odkhuu, D.; Park, N.; Cho, J.; Shin, H. S. Synthesis and characterization of patronite form of vanadium sulfide on graphitic layer. *J. Am. Chem. Soc.* **2013**, *135*, 8720−8725.
(25) Wang, S. Z.; Gong, F.; Yang, S. Z.; Liao, J. X.; Wu, M. Q.; Xu, Z. Q.; Chen, C.; Yang, X. F.; Zhao, F. P.; Wang, B.; et al. Graphene Oxide-Template Controlled Cuboid-Shaped High-Capacity VS_4 Nanoparticles as Anode for Sodium-Ion Batteries. *Adv. Funct. Mater.* **2018**, *28*, 1801806.
(26) Wang, S. Z.; Liao, J. X.; Wu, M. Q.; Xu, Z. Q.; Gong, F.; Chen, C.; Wang, Y. S.; Yan, X. B. High Rate and Long Cycle Life of a CNT/rGO/Si Nanoparticle Composite Anode for Lithium-Ion Batteries. *Part. Part. Syst. Charact.* **2017**, *34*, 1700141.
(27) Song, Y.; Liao, J.; Chen, C.; Yang, J.; Chen, J.; Gong, F.; Wang, S.; Xu, Z.; Wu, M. Controllable morphologies and electrochemical performances of self-assembled nano-honeycomb WS_2 anodes modified by graphene doping for lithium and sodium ion batteries. *Carbon* **2019**, *142*, 697−706.
(28) Chen, Y.; Xie, K.; Liu, Z. X. Determination of the position of V^{4+} as minor component in XPS spectra by difference spectra. *Appl. Surf. Sci.* **1998**, *133*, 221−224.
(29) Mendialdua, J.; Casanova, R.; Barbaux, Y. XPS studies of V_2O_5, V_6O_{13}, VO_2 and V_2O_3. *J. Electron Spectrosc. Relat. Phenom.* **1995**, *71*, 249−261.
(30) Chastain, J.; King, R. C.; Moulder, J. *Handbook of X-ray photoelectron spectroscopy: a reference book of standard spectra for identification and interpretation of XPS data*; Physical Electronics Division, Perkin-Elmer Corporation: Eden Prairie, MN, 1992.
(31) Jeong, Y.; Kim, J.; Kwon, S.; Oh, J.; Park, J.; Jung, Y.; Lee, S.; Yang, S.; Park, C. Rational design of exfoliated 1T MoS_2@CNT-based bifunctional separators for lithium sulfur batteries. *J. Mater. Chem. A* **2017**, *5*, 23909−23918.
(32) Ponraj, R.; Kannan, A. G.; Ahn, J. H.; Lee, J. H.; Kang, J.; Han, B.; Kim, D.-W. Effective Trapping of Lithium Polysulfides Using a Functionalized Carbon Nanotube-Coated Separator for Lithium−Sulfur Cells with Enhanced Cycling Stability. *ACS Appl. Mater. Interfaces* **2017**, *9*, 38445−38454.
(33) Zhang, Q.; Wang, Y.; Seh, Z. W.; Fu, Z.; Zhang, R.; Cui, Y. Understanding the Anchoring Effect of Two-Dimensional Layered Materials for Lithium−Sulfur Batteries. *Nano Lett.* **2015**, *15*, 3780−3786.
(34) Hu, L.; Dai, C.; Lim, J. M.; Chen, Y.; Lian, X.; Wang, M.; Li, Y.; Xiao, P.; Henkelman, G.; Xu, M. A highly efficient double-hierarchical sulfur host for advanced lithium-sulfur batteries. *Chem. Sci.* **2018**, *9*, 666−675.
(35) Song, Y.; Zhao, W.; Zhu, X.; Zhang, L.; Li, Q.; Ding, F.; Liu, Z.; Sun, J. Vanadium Dioxide-Graphene Composite with Ultrafast Anchoring Behavior of Polysulfides for Lithium-Sulfur Batteries. *ACS Appl. Mater. Interfaces* **2018**, *10*, 15733−15741.
(36) Song, Y.; Zhao, W.; Kong, L.; Zhang, L.; Zhu, X.; Shao, Y.; Ding, F.; Zhang, Q.; Sun, J.; Liu, Z. Synchronous immobilization and conversion of polysulfides on a VO_2−VN binary host targeting high sulfur load Li−S batteries. *Energy Environ. Sci.* **2018**, *11*, 2620−2630.
(37) Song, Y.; Zhao, W.; Wei, N.; Zhang, L.; Ding, F.; Liu, Z.; Sun, J. In-situ PECVD-enabled graphene-V_2O_3 hybrid host for lithium−sulfur batteries. *Nano Energy* **2018**, *53*, 432−439.
(38) Peng, H.-J.; Zhang, G.; Chen, X.; Zhang, Z.-W.; Xu, W.-T.; Huang, J.-Q.; Zhang, Q. Enhanced Electrochemical Kinetics on Conductive Polar Mediators for Lithium-Sulfur Batteries. *Angew. Chem., Int. Ed.* **2016**, *55*, 12990−12995.
(39) Zhou, T.; Lv, W.; Li, J.; Zhou, G.; Zhao, Y.; Fan, S.; Liu, B.; Li, B.; Kang, F.; Yang, Q.-H. Twinborn TiO_2−TiN heterostructures enabling smooth trapping−diffusion−conversion of polysulfides towards ultralong life lithium−sulfur batteries. *Energy Environ. Sci.* **2017**, *10*, 1694−1703.
(40) Wang, S.; Liao, J.; Yang, X.; Liang, J.; Sun, Q.; Liang, J.; Zhao, F.; Koo, A.; Kong, F.; Yao, Y.; et al. Designing a highly efficient polysulfide conversion catalyst with paramontroseite for high-performance and long-life lithium-sulfur batteries. *Nano Energy* **2019**, *57*, 230−240.
(41) Zhong, Y.; Chao, D.; Deng, S.; Zhan, J.; Fang, R.; Xia, Y.; Wang, Y.; Wang, X.; Xia, X.; Tu, J. Confining Sulfur in Integrated Composite Scaffold with Highly Porous Carbon Fibers/Vanadium Nitride Arrays for High-Performance Lithium-Sulfur Batteries. *Adv. Funct. Mater.* **2018**, *28*, 1706391.
(42) Zhou, G.; Tian, H.; Jin, Y.; Tao, X.; Liu, B.; Zhang, R.; Seh, Z. W.; Zhuo, D.; Liu, Y.; Sun, J.; et al. Catalytic oxidation of Li_2S on the surface of metal sulfides for Li-S batteries. *Proc. Natl. Acad. Sci. U. S. A.* **2017**, *114*, 840−845.
(43) Xu, K.; Liu, X.; Liang, J.; Cai, J.; Zhang, K.; Lu, Y.; Wu, X.; Zhu, M.; Liu, Y.; Zhu, Y.; et al. Manipulating the Redox Kinetics of Li−S Chemistry by Tellurium Doping for Improved Li−S Batteries. *ACS Energy Lett.* **2018**, *3*, 420−427.

DOI: 10.1021/acsenergylett.9b00076
ACS Energy Lett. 2019, 4, 755−762